

---

# HIERARCHICAL AND STEP-LAYER-WISE TUNING OF ATTENTION SPECIALTY FOR MULTI-INSTANCE SYNTHESIS IN DIFFUSION TRANSFORMERS

---

**Chunyang Zhang**<sup>†</sup>

School of Systems and Computing  
University of New South Wales  
Canberra, ACT 2612, Australia  
chunyang.zhang@unsw.edu.au

**Zhenhong Sun**<sup>†‡</sup>

School of Engineering  
Australian National University  
Canberra, ACT 2601, Australia  
zhenhongsun1992@outlook.com

**Zhicheng Zhang**

School of Business  
University of New South Wales  
Canberra, ACT 2612, Australia  
zhicheng.zhang2@unsw.edu.au

**Junyan Wang**

Australian Institute for Machine Learning  
University of Adelaide  
Adelaide, SA 5371, Australia  
junyan.wang@adelaide.edu.au

**Yu Zhang**

School of Business  
University of New South Wales  
Canberra, ACT 2612, Australia  
m.yuzhang@unsw.edu.au

**Dong Gong**

School of Computer Science and Engineering  
University of New South Wales  
Sydney, NSW 2052, Australia  
dong.gong@unsw.edu.au

**Huadong Mo**\*

School of Systems and Computing  
University of New South Wales  
Canberra, ACT 2612, Australia  
huadong.mo@unsw.edu.au

**Daoyi Dong**\*

School of Computer Science  
University of Technology Sydney  
Sydney, NSW 2007, Australia  
daoyi.dong@uts.edu.au

## ABSTRACT

Text-to-image (T2I) generation models often struggle with multi-instance synthesis (MIS), where they must accurately depict multiple distinct instances in a single image based on complex prompts detailing individual features. Traditional MIS control methods for UNet architectures like SD v1.5/SDXL fail to adapt to DiT-based models like FLUX and SD v3.5, which rely on integrated attention between image and text tokens rather than text-image cross-attention. To enhance MIS in DiT, we first analyze the mixed attention mechanism in DiT. Our token-wise and layer-wise analysis of attention maps reveals a hierarchical response structure: instance tokens dominate early layers, background tokens in middle layers, and attribute tokens in later layers. Building on this observation, we propose a training-free approach for enhancing MIS in DiT-based models with hierarchical and step-layer-wise attention specialty tuning (AST). AST amplifies key regions while suppressing irrelevant areas in distinct attention maps across layers and steps, guided by the hierarchical structure. This optimizes multimodal interactions by hierarchically decoupling the complex prompts with instance-based sketches. We evaluate our approach using upgraded sketch-based layouts for the T2I-CompBench and customized complex scenes. Both quantitative and qualitative results confirm our method enhances complex layout generation, ensuring precise instance placement and attribute representation in MIS.

---

\*Corresponding Authors; <sup>†</sup>Equal Contribution; <sup>‡</sup>Project Leader.

# 1 Introduction

Multi-instance synthesis (MIS) is a key challenge in text-to-image (T2I) generation, essential for enabling generative models’ real-world applications [1, 2, 3, 4, 5, 6]. It focuses on accurately representing multiple distinct instances within a single image, responding precisely to complex prompts that specify individual features for each instance. Leveraging UNet-based diffusion models (e.g., SD v1.5 [7] and SDXL [8]), current generative models [1, 2, 3, 9, 4, 5, 6, 10, 11, 12, 13, 14, 15, 16, 17] typically adopt a divide-and-conquer approach to enhance MIS by processing instances and attributes separately, employing either fine-tuning or training-free methods. Fine-tuning leverages task-specific data to enhance synthesis quality but demands extensive resources for data collection and training, while training-free methods utilize inherent model capabilities offering flexible adaptability, and low computational cost, making them a desirable approach for practical MIS applications. Recently, Diffusion Transformer (DiT)-based models such as FLUX [18] and SD v3.5 [19] have demonstrated significant advances in text-image consistency and high-quality image generation. Transitioning from traditional UNet architectures with cross-attention mechanisms to more sophisticated DiT architectures [20] utilizing combined attention mechanisms has notably improved complex prompt handling and image representation. However, these enhancements have not explicitly targeted improvements for MIS, especially in scenarios involving intricate prompts and complex spatial layouts. Moreover, this transition further complicates the application of existing training-free approaches, which were initially designed around UNet architectures. Consequently, the emerging shift also highlights a pressing need to investigate attention mechanisms tailored specifically for DiT architectures that can facilitate effective training-free solutions for MIS tasks.

The DiT architecture replaces traditional self- and cross-attention with a unified attention, and injects text embeddings at each inference step, enabling consistent fusion of textual and visual information. To explore this mechanism, we analyze specific attention dynamics, focusing on text-to-text (T2T), image-to-image (I2I), and image-to-text (I2T) interactions. Attention map analysis reveals hierarchical responses: instance tokens dominate early layers, background tokens in middle layers, and attribute tokens in later layers, with critical integration mostly in early inference steps. A step-layer-wise token-exchange experiment further examines the DiT’s text embeddings interaction by swapping background, attribute, and instance tokens at specific layers and steps, which confirms the above hierarchical attention responses. Collectively, these analyses clarify the specific roles of various tokens and provide valuable insights, forming a strong foundation for developing controlled MIS.

Building on the outlined observations, we propose a training-free approach for enhancing MIS in DiT models with hierarchical and step-layer-wise **Attention Specialty Tuning (AST)**, focusing on the crucial role of attention maps. Specifically, AST employs a unified scalable module with specialized masks to improve the attention distribution for distinct T2T, I2I, and I2T attentions. It enhances synthesis by selectively amplifying key regions and suppressing irrelevant areas in attention maps, improving alignment between specific textual or visual regions for enhanced details. **Hierarchical and Step-Layer-Wise (HSLW)** module refines alignment by modulating attention across layers and steps, designating specific layers for attributes, instances, and background hierarchically, which optimizes multimodal interactions within T2T, I2I, and I2T modules by hierarchically decoupling the complex prompts with instance-based sketches. Meanwhile, we introduce an upgrade patch with sketch-based layouts for the T2I-CompBench [21] and customized complex scenes to evaluate the performance, where our method achieves accurate instance placement and attribute representation for complex layouts in the MIS. The contributions of our work are outlined as follows:

- We explore the mixed attention mechanism of the DiT model and design the token exchange experiment, revealing the influence of hierarchical attention responses.
- HSLW-based AST highlights key regions and suppresses irrelevant areas across layers and steps, optimizing multimodal interactions via instance-based sketches.
- Benefiting from AST, our model extends the DiTs with an improved fusion of textual and visual representations, realizing high-quality MIS.

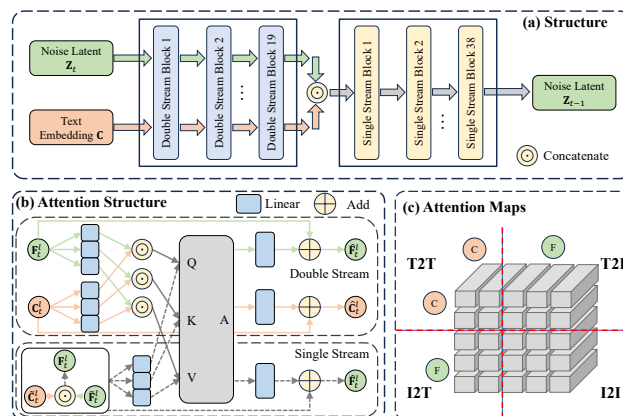


Figure 1: Schematic architecture of the DiT-based models (a) with double/single-stream attentions (b). The attention map in (c) reveals four distinct interaction patterns: text-to-text, text-to-image, image-to-text, and image-to-image, enabling deep consistent fusion between text and tokens.

## 2 Related Work

**T2I Synthesis.** Diffusion models [22, 23, 24, 25, 26] have shown remarkable performance in generating high-quality images for T2I synthesis and editing [27, 28]. Latent Diffusion Models (LDMs) [7] further enhance both diversity and realism while maintaining low computational complexity, utilizing the Variational AutoEncoder [29] and UNet architecture [30] with a cross-attention mechanism. Recently, unified transformer-based models [20, 31, 19, 32, 18] represented by DiT [20], combined with the rectified flow technique [33, 19], are increasingly demonstrating their superiority compared with UNet architecture. Notably, DiT models have achieved new state-of-the-art performance in image synthesis. However, the DiT-based models face challenges in controllable MIS when dealing with complex prompts and specific layouts.

**Multi-Instance Synthesis.** MIS focuses on accurately generating images containing multiple distinct instances that align with specific attributes and layouts [34, 1, 2, 3, 9, 4, 5, 6, 10, 11, 12, 13, 14, 15, 16, 17]. Based on the type of layout input, methods can be divided into bounding box-based [2, 3, 9, 4, 5, 10, 11, 12, 6, 34, 13, 14] and sketch-based [1, 15, 16, 17, 35] approaches. Also, these methods can be further classified into fine-tuning methods that leverage formatted data [2, 3, 9, 4, 5, 10, 11, 12, 15, 16, 17] and training-free methods that use cross-attention mechanisms directly [6, 34, 13, 14, 1, 36]. Adapting fine-tuning on the DiT-based models could improve MIS, but the high computational costs make a training-free method more efficient. Unlike bounding box layouts, sketch layouts offer flexible shapes and semantic details, making them accessible to a wider non-artistic audience. Therefore, we aim to develop a training-free method using sketch layouts on the DiT-based models for effective MIS.

**Attention Tuning Synthesis.** In the UNet architecture with the cross attention mechanism, works [37, 38, 39, 40, 41, 42] use tuning strategies to refine attention maps, guiding the generation process and enhancing the model’s accuracy in following prompts. For example, Prompt-to-Prompt [37] examines attention maps and introduces training-free attention tuning to improve alignment between textual prompts and specified instances. P+ [43] manipulates prompt token replacement across layers to reveal each layer’s influence on token behavior, while the HCP model [42] illustrates how tokens react differently at various inference steps. Meanwhile, Dense Diffusion [1] uses sketch layouts to target specific regions, adjusting self- and cross-attention maps during denoising to enhance image generation. However, as the focus shifts to DiT-based models, traditional methods effective in the UNet architecture face challenges, which underscores the need to explore new tuning mechanisms within DiT to develop an efficient training-free approach.

## 3 Proposed Approach

In this section, our approach begins with an examination of the DiT-based model, emphasizing the role of new attention mechanisms. Following this analysis, we design a step-layer-wise token-exchange experiment to investigate prompt token replacement across layers. Subsequently, we propose a training-free HSLW module of AST for MIS with DiT-based models, followed by detailed explanations.

### 3.1 Preliminary

Unlike the traditional UNet structure, the DiT architecture [20] eliminates spatial downsampling and upsampling to sustain a consistent higher spatial dimension. It substitutes the original self- and cross-attention mechanisms with a unified attention mechanism, simplifying the architecture, enhancing efficiency, and improving generalization effectiveness [20, 19, 18]. Instead of injecting text embeddings via cross-attention at each layer, the DiT-based model introduces them once at the start of each inference step, allowing them to merge with the noise latent for deeper and spatially consistent text-visual fusion, as shown in Figure 1. The DiT-based model employs double stream blocks that initially combine latent and text embeddings through separate streams, followed by single stream blocks that unify them into a single stream, as illustrated in Figure 1 (a). Despite the structural differences of the two streams, they adhere to a new attention mechanism, with the intermediate output feature  $\tilde{\mathbf{F}}_t^l$  defined by:

$$\tilde{\mathbf{F}}_t^l = \mathbf{A}_t^l \mathbf{V}_t^l = \text{softmax} \left( \frac{\mathbf{Q}_t^l \mathbf{K}_t^{lT}}{\sqrt{d_c^l + d_z^l}} \right) \mathbf{V}_t^l, \quad (1)$$

where  $\mathbf{Q}_t^l$ ,  $\mathbf{K}_t^l$  and  $\mathbf{V}_t^l$  reside in the dimension of  $\mathbb{R}^{(d_c+hw) \times d^l}$ , transformed by the linear layers from the latent features and text embeddings, as depicted in Figure 1 (b). Here,  $d_c$  represents the max tokens of text embeddings,  $hw$  is the spatial dimensions, and  $d^l$  is the embedding dimension of linear layers. Consequently, the attention maps  $\mathbf{A}_t^l \in \mathbb{R}^{(d_c+hw) \times (d_c+hw)}$  are divided into four parts (Figure 1 (c)), covering T2T, T2I, I2T and I2I modules. This architecture functions as an equivalent blend of the original self- and cross-attention, improving text-visual fusion.

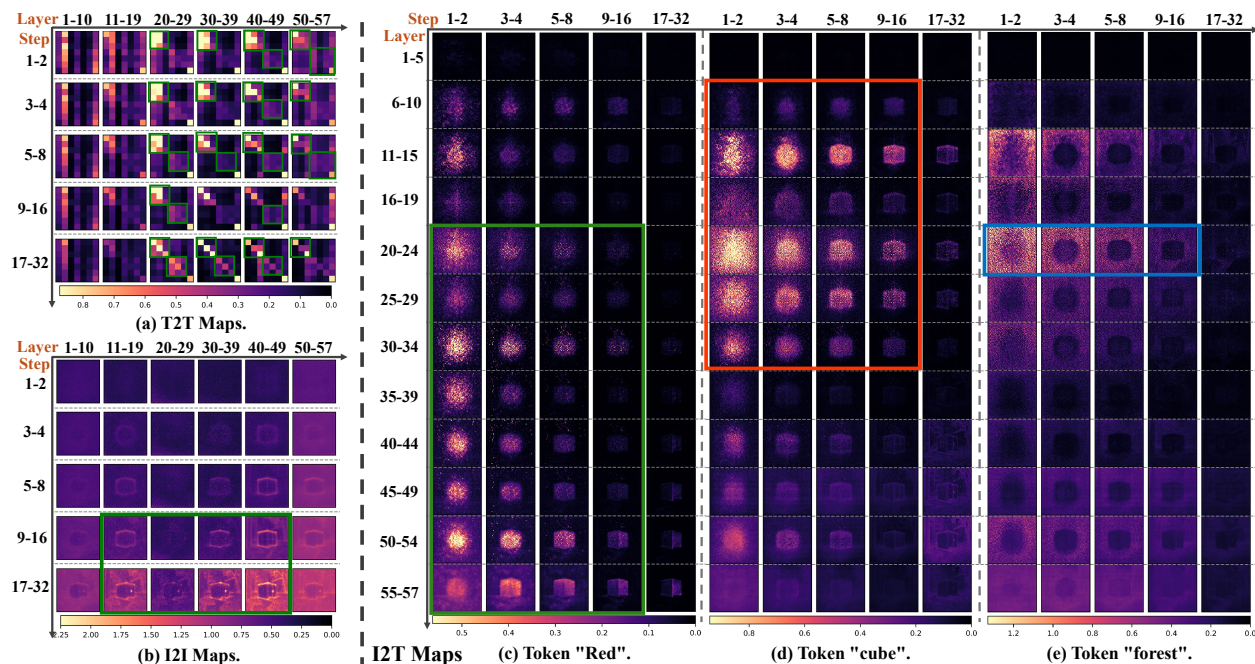


Figure 2: Attention map averages for the prompt “Red cube in a forest”. (a) T2T maps show strong intra-segment interactions within valid tokens of “Red cube” (first 3 tokens) and “in a forest” (last 4 tokens). (b) I2I maps (the maximum value of each point relative to all other points) reveal growing interaction between “Red cube” and “a forest” segments over steps. (c/d/e) I2T attention maps on individual tokens highlight that instance tokens dominate early layers, background tokens in the middle, and color tokens later, with most information integrated in the first half of steps. T2I maps showing lower scores with weak impact and more examples are present in the **Appendix.8**.

### 3.2 Attention Analysis of DiT Model

**Hierarchical Attention Responses.** Following the analytical approaches [37, 42] based on the UNet architecture, we utilize the prompt “Red cube in a forest” to examine the functionality of four regions in the attention maps within the DiT-based model. For simplicity, we introduce a prompt that includes an instance with an attribute alongside a background element, allowing an intuitive investigation. The visualization maps are categorized by types as shown in Figure 2: self-attention maps (T2T and I2I), and cross-attention-based I2T maps. Notably, the T2I attention shows lower attention scores relative to others, indicating a weak impact on generation, which is provided in **Appendix.8**. We have the following observation.

**1) Text-to-Text:** This region enhances intra-segment correlations while minimizing inter-segment interference. Specifically, “Red cube” (3 tokens) and “in a forest”(4 tokens) show high internal attention scores, indicating strong token interactions within each sub-prompt, supporting instance-specific responses, and decreasing cross-attribute coupling.

**2) Image-to-Image.** This region controls the interactions of instances, allowing elements like the “cube” and “forest” to emerge through denoising gradually. Early stages focus on the instance’s internal structure, while later stages increase interaction with the background, suggesting that interventions in the instance are most effective in early stages.

**3) Image-to-Text.** This region distinguishes instances with attributes and background activating at different but early stages: the attribute “Red” in layers 20-57, the instance “cube” in layers 6-34, and the background “forest” in layers 20-24. This step-layer-wise distribution suggests a precise scope for attention manipulation, particularly in layers where background and instance overlap, allowing for targeted adjustments to realize high efficiency.

In summary, this analysis reveals that HSLW attention specificity in I2T enhance text responsiveness in the text-to-query region while defining semantic and structural features in the image-to-query region. This enables DiT-based model to generate coherent images, integrating foreground instances with attributes into the background and providing key priors for attention manipulation.

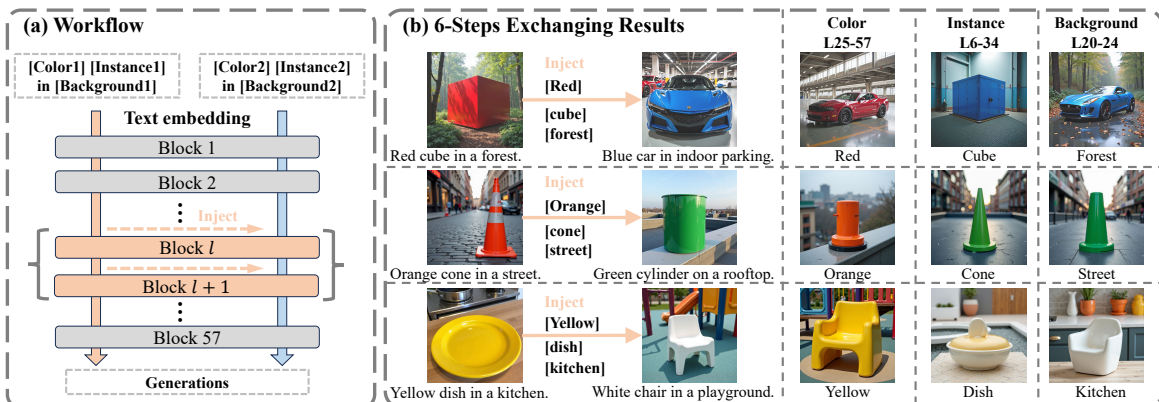


Figure 3: Step-Layer-Wise Token Exchange involved injecting specific tokens between two prompts formatted as “[color] [Instance] in [Background]” (a). First 6-step exchanging results show that specific token concept can be replaced in certain layers (e.g., L25-27) with other concepts preserving, aligning with the hierarchical attention responses in Figure 2. Step-wise visualization is detailed in **Appendix.9**.

**Step-Layer-Wise Token Exchanging.** As mentioned in Sec. 3.1, the DiT model introduces text embeddings once at the start of each inference, allowing them to flow alongside the noise latent. This structure supports enhanced integration of textual and visual information at a uniform spatial scale, although its underlying role remains unexamined. Inspired by the P+ model [43], which manipulates prompt token replacement across layers, we propose a step-layer-wise token exchanging. The exchange involved injecting specific tokens at different layers between two prompts formatted as “[color] [Instance] in [Background]”, to observe the evolution of text embeddings during diffusion (Figure 3 (a)). The resulting images in Figure 3 (b) demonstrate that selective component replacements, such as color, instance, and background, operate on different layers, supporting our earlier findings on hierarchical attention responses and step-layer-wise specificity in I2T module. For instance, elements such as “red”, “cube”, and “forest” prominently emerge by step 6 in a harmonious style with other concepts preserving. These findings provide a foundation for developing an attention tuning on the DiT model for controllable MIS with complex prompts and layouts.

### 3.3 Hierarchical Tuning

To address the challenges of the attention mechanism discussed in Section 3.2, we propose a training-free hierarchical tuning strategy, which leverages the strengths of the pre-trained DiT-based model with hierarchical and step-layer-wise AST, incorporating: textual prompts  $\mathbf{c}$  and corresponding sketch images  $\mathbf{S}$ , as shown in Figure 4 .

**Attention Specialty Tuning.** The essence of attention tuning in the cross-attention mechanism is to enhance the values of meaningful regions in the attention maps while attenuating the values of weak or non-meaningful regions [37, 43, 1, 42]. However, the DiT-based models’ attention mechanism comprises self-focused T2T and I2I, as well as cross-focused I2T and T2I attention maps, each exhibiting unique characteristics that influence generation outcomes. Therefore, effective attention tuning of DiT-based models requires accounting for these variations to enhance instance accuracy and detail in MIS. Thus, we propose a plug-in strategy for the mixed attention mechanism shown in Figure 4 (b), named AST.

We design a unified scalable module to process different attention types consistently. Adjustments are focused on mask specification to enhance or attenuate specific regions within each attention category. This unified structure streamlines processing across attention types, improving model efficiency, scalability, and adaptability in highlighting meaningful regions. The process of tuning original attention map  $\mathbf{A}_t^l$  (after softmax) is specified as follows:

$$\hat{\mathbf{A}}_t^l = f_{norm}(\mathbf{A}_t^l \odot \exp(\beta_t \cdot \mathbf{G} \odot (\mathbf{M} - \mathbf{A}_t^l))), \quad (2)$$

where  $\hat{\mathbf{A}}_t^l$  represents the tuned attention maps at layer  $l$  and time step  $t$ , and  $\odot$  denotes element-wise multiplication (Comparison before softmax is in **Appendix.7**).  $f_{norm}(\mathbf{B}) = \mathbf{B} / \sum_i B_i$  is the weight normalization to form a distribution summing to 1 along the embedding dimension. Here,  $\beta_t = \lambda(t/T)^4$  is a scaling factor that adjusts the sensitivity of the enhancement with a hyper-parameter  $\lambda$  and maximum  $T$  steps.  $\mathbf{G}$  is a sensitivity matrix to modulate region-specific adjustments (following Dense Diffusion [1], the specific formula is provided in **Appendix.3**), with values determined by the proportion of the sketch area relative to the overall image area—smaller objects approach 1, while larger objects approach 0. Notably,  $\mathbf{M}$  is the mask matrix specific to different attention types, incorporating

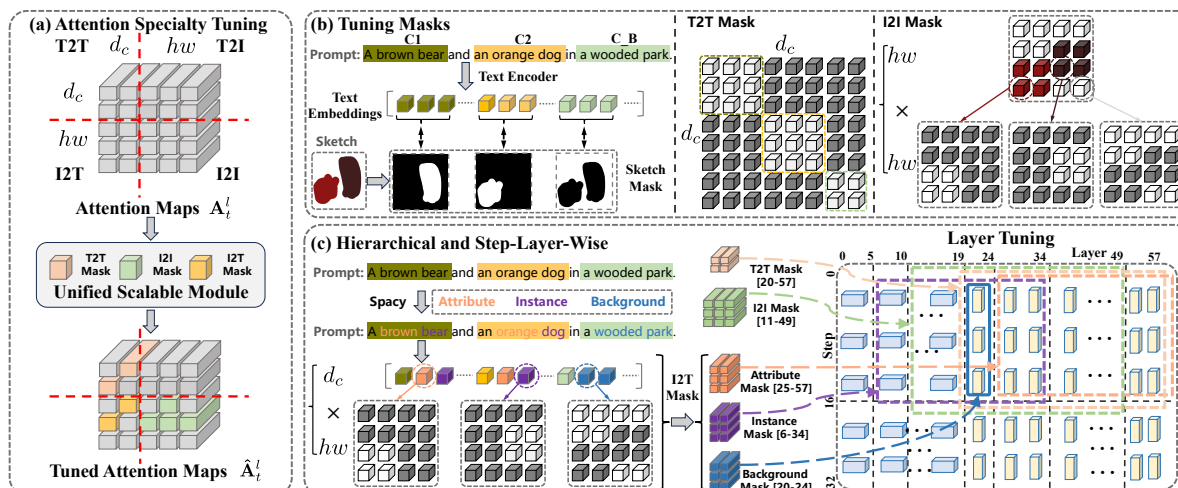


Figure 4: Overview of the hierarchical tuning strategy for DiT models. (a) Attention specialty tuning enhances meaningful regions while suppressing non-meaningful ones via a unified scalable module with distinct tuning masks. (b) Tuning masks for T2T and I2I masks are directly built from prompt segments and sketches. (c) Hierarchical and step-layer-wise module refines alignment by adjusting each component’s impact across specific layers and steps, assigning layers for attributes, instances, and background tokens within first 16 steps.

conditions corresponding to prompts  $\mathbf{c} = \{c_1, c_2, \dots, c_N\}$  and sketch images  $\mathbf{S} = \{S_1, S_2, \dots, S_N\}$  ( $N$  is the number of sub-prompts), and guiding adjustments to attention values. Relying on the characteristics of the attention maps, each attention employs distinct constructions:

1) **T2T Mask**: In the attention maps, the T2T region (sized  $d_c \times d_c$ ) represents the correlation between elements within the text embeddings. To strengthen the coupling among sub-prompt elements, as concluded in Section 3.2, we apply a binary mask matrix within sub-prompts, as shown in Figure 4 (b), and expressed by:

$$\mathbf{M}_{T2T}(i, j) = 1 \quad \text{if } i, j \in \mathbf{c}_k, \quad k \in \{1, \dots, N\}. \quad (3)$$

2) **I2I Mask**: I2I region ( $hw \times hw$ ) captures correlations between each element and all others, promoting internal coherence across image features. Therefore, the mask should represent the alignment of visual elements within a sub-prompt instance (Figure 4 (b)), reinforcing the associations within the instance, and is calculated as:

$$\mathbf{M}_{I2I}(i, j) = 1 \quad \text{if } i, j \in S_k. \quad (4)$$

3) **I2T Mask**: I2T region ( $hw \times d_c$ ) represents the alignment between image and text embeddings. For each text embedding corresponding to sub-prompts, attention values should be enhanced at positions that align with the corresponding sketch locations in latent space (Figure 4 (c)), reinforcing cross-modal correspondence between visual features and textual elements within the prompts, defined by:

$$\mathbf{M}_{I2T}(i, j) = 1 \quad \text{if } i \in S_k \text{ and } j \in \mathbf{c}_k. \quad (5)$$

**Hierarchical and Step-Layer-Wise Module.** HSLW module of different attention types effectively handles the coupled alignment of textual information and visual layout across different instances, especially for T2T and I2I. However, the I2T module, which ultimately governs multimodal interaction, lacks sufficient details in tuning. As discussed in Section 3.2, the background, instance, and attribute are coupled in the spatial dimension but have distinct regions of influence (Figure 2 (c)). Thus, a step-layer-wise modulation for I2T focusing on background, instance, and attribute is introduced to better respond to textual information for each instance.

Specifically, for different sub-prompts, we employ an NLP library (e.g., SpaCy) to distinguish between adjectives (attributes) and nouns (instances) words. Adjectives and instance words classified as background words are marked by their respective index positions in the text embedding. Corresponding to the hierarchical attention responses, an instance tuning is applied to the earlier layers (layers 6 to 34), a background tuning is incorporated into the intermediate layers (layers 20 to 24) while a attribute tuning is applied to the later layers of the network (layers 25 to 57), as shown in Figure 4 (c). This hierarchical allocation of I2T layers helps achieve a more precise alignment between textual and visual information in complex prompts, improving the response of MIS. Moreover, distinct steps and layers are applied

for T2T and I2I to analyze the self-focused components, as illustrated in Figure 2. T2T attention should be emphasized in layers 20 to 57 to enhance intra-segment token interactions and avoid attribute and instance leakage due to strong correlations in the first 16 steps. Similarly, I2I attention should be refined in the early layers (11 to 49) to better capture the layout relationships between background and foreground instances.

## 4 Experiments

Table 1: Evaluation results on T2I-CompBench with upgraded sketches (**Appendix.5**) and image quality assessment on customized complex cases (**Appendix.6**) with study scores (1-5) and ImageReward [44]. ImageReward shows that fine-tuning the base model degrades image quality usually, whereas our method results in a slight drop compared with others. # denotes results from T2I-CompBench, while others are re-evaluated. Inference time is measured with identical 50 denoising steps. “Ours-v1” indicates FLUX with I2T mask, “Ours-v2” indicates FLUX with I2T+I2I masks and “Ours-v3” indicates FLUX with I2T+T2T mask.

Metrics	T2I-CompBench			Customized Cases		
	Color B-VQA $\uparrow$	2D Spatial UniDet $\uparrow$	Complex 3 in 1 $\uparrow$	User Study $\uparrow$	Image Reward $\uparrow$	Infer s/it
SD v1.5# [7]	0.3765	0.1246	0.3080	1.74	-0.448	7
SD v2# [7]	0.5065	0.1342	0.3386	2.21	-0.1482	6
SDXL# [8]	0.6369	0.2032	0.3237	2.76	0.48	14
Pixart# [31]	0.6690	0.2064	0.3433	3.01	0.8584	14
SD v3.5 [19]	0.7484	0.3231	0.5334	3.29	1.4592	62
FLUX-dev [18]	0.7398	0.2589	0.5081	3.26	1.2371	23
DenseDiff [1]	0.4316	0.2142	0.3563	2.17	-0.352	12
BoxDiff [6]	0.5146	0.2582	0.4044	1.76	-0.3402	10
Atten-Refoc [12]	0.4442	0.4503	0.3966	2.21	-0.0564	37
HiCO [45]	0.5500	0.3181	0.4274	2.42	-0.1865	10
R&B [46]	0.5069	0.3841	0.4204	1.86	-0.6838	40
GrounDiT [47]	0.5997	0.4409	0.5031	2.71	0.5521	130
MIGC [10]	0.4974	0.4628	0.4974	2.48	-0.184	9
Instance [17]	0.6583	0.4623	0.5059	3.14	0.1888	14
RPG [14]	0.4724	0.2517	0.3850	3.01	0.0277	20
Ours+SD v3.5	0.7531	0.4188	0.5567	3.63	1.3257	94
Ours+FLUX	0.7822	0.5004	0.5717	4.03	0.9213	29
Ours-v1	0.7459	0.4383	0.5456	3.41	0.8943	29
Ours-v2	0.7854	0.4569	0.5654	3.61	0.7788	29
Ours-v3	0.7853	0.4403	0.5619	3.76	0.8338	29

### 4.1 Implementation Details

**Baselines and Settings.** In our experiments, we utilize the FLUX-dev model [18] as both the analysis and evaluation model, and SD v3.5 [19] as the evaluation model. The hyperparameters  $\lambda$  in Eq. (2) are set to  $\lambda_{cross} = 5.0$  and  $\lambda_{self} = 3.5$ . During inference, we apply the default Euler Discrete Scheduler [19] with 32 steps and a guidance scale of 7 at a resolution of  $1024 \times 1024$ . Inferences are conducted on 1 Nvidia V100 GPU with 32 GB of memory, while analysis experiments are performed on 1 A100 GPU with 80 GB of memory to accommodate the storage of attention maps sized  $4608 \times 4608$ . To evaluate our method, we compare it against several baseline models, including SD v1.5 [7], SD v2[7], SDXL [8], and Pixart [8], and related training-free/based methods, including DenseDiff [1], BoxDiff [6], Atten-Refoc [12], HiCO [45], R&B [46], GrounDiT [47], MIGC [10], Instance [17], and RPG [14].

**Datasets and Metrics.** The T2I-CompBench [49] is used to evaluate the MIS capability in terms of attribute binding, instance placement, and complex relationships using several criteria, including B-VQA [50], UniDet [51], and CLIP-Score [52]. As our method requires preliminary sketch information in advance, we utilize GPT-4V [48] to generate sketch images that automatically segment each instance and output the associated sketch mask (Details in **Appendix.5**). To further assess our method’s ability to handle extreme complexity, we customized 20 complex scenes with 6-8 instances and varying attributes to evaluate overall image quality (Details in **Appendix.6**). After the multimedia

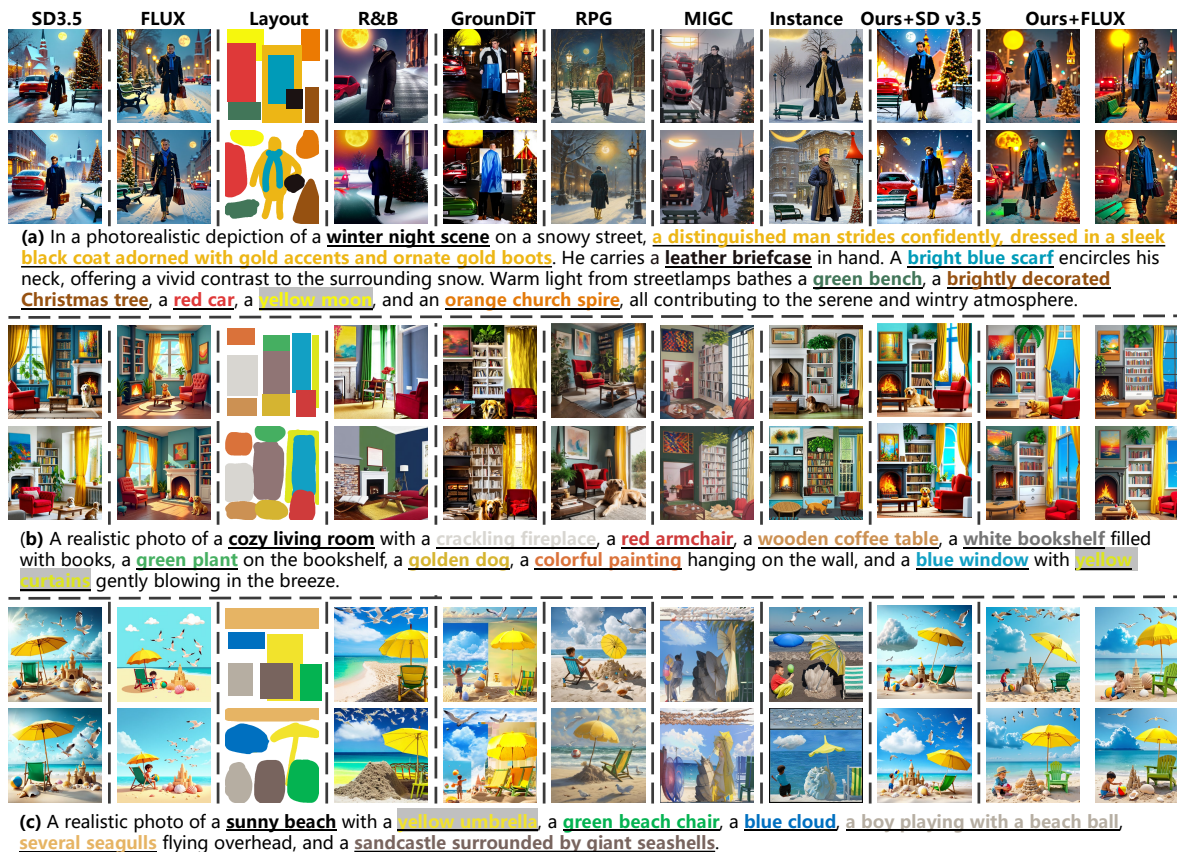


Figure 5: Visualizations on customized complex cases (More examples are in **Appendix.6**). Bounding box layouts are for MIGC [10] Instance [17], R&B [46], and GrounDiT [47], and the layout of RPG [14] is generated by the GPT-4o [48], while sketch layouts are for ours. Our approach extends DiT models (SD v3.5 and FLUX) with better multi-instance alignment with prompts and sketch-based layouts. The underlined prompts within the prompts are the sub-prompts for instances, with colors matching those in the sketch.

subjective testing [53], we conducted a human assessment using a 1-5 rating scale for image quality, placement, and prompt-image consistency. Additionally, we used a pre-trained human preference model ImageReward [44] to assess the aesthetic quality of images.

## 4.2 Main Results

**Quantitative Evaluation.** We conduct quantitative evaluations on T2I-CompBench with upgraded sketches (**Appendix.5**) and image quality assessment on customized complex cases (**Appendix.6**) with study scores (1-5) and ImageReward [44], shown in Table 1. The results on T2I-CompBench indicate that our tuning strategy extends the base models with superior performance across all three scenarios, demonstrating exceptional generative capability in both layout and attribute synthesis and consistency with the findings in Section 3.2 regarding the unified attention mechanism. AST module refines cross-focus and self-focus attention for better prompt responsiveness, while HSLW tuning ensures each instance aligns with its corresponding attribute. The user study results in Table 1 highlight improvements in generating human-preferred images for multi-instance scenarios over image quality, placement, and prompt-image consistency. Notably, ImageReward scores for aesthetic quality of images provide another insight that training-based/free methods typically show performance degradation relative to their baselines due to the distribution transferring, but our method maintains near-baseline performance with only slight decreases compared to SD v3.5 and FLUX. These quantitative results collectively demonstrate our method’s effectiveness in enhancing DiT-based models capabilities for accurate instance placement and attribute representation in MIS.



**Qualitative Evaluation.** In the MIS comparison, we employ three complex prompts, each specifying over eight distinct instances with unique attributes (More examples are in Appendix.6). Figure 5 demonstrates that our method achieves superior precision in rendering multiple instances with designated attributes, maintaining sketch constraints and cohesive background-foreground integration. For instance, “an orange church spire” in (a) and “blue window” in (b) match the layout and specified color attributes precisely; similarly, “blue cloud” and “green beach chair” in (c) conform precisely to the textual descriptions and layout constraints. Furthermore, we designed additional test cases featuring multiple repeated small instances and occluded instances to validate our method’s capability in handling extreme complexity, as shown in Figure 6. The results demonstrate our method’s effectiveness in: (1) numerous instances with varying sizes and colors (e.g., multiple flowers and differently sized/colored mushrooms in (a)); (2) complex spatial relationships (e.g., five basketballs with varying attributes in (b)); (3) intricate occlusion scenarios (e.g., cats before/after a table in (c), and a hamster on top of a mushroom in (d)). These findings collectively demonstrate our method’s robust capability for accurate instance placement and attribute representation under complex multi-instance sketch constraints.



Figure 6: Visualization of handling small/repeated instances (“flower”, “mushroom”, “basketball”) and occluded instances (“apples and bananas in plates”, “cat in front/behind table”, “leaf on log”, “hamster on mushroom”).

### 4.3 Ablation Study and Analysis

#### Module Comparison.

Figure 7 shows visualization results, with attribute and position inaccuracies highlighted in colored boxes. The data reveals three main findings: (1) The single I2T tuning strategy can generate all instances but lacks precise positioning, as seen in examples like the “Christmas tree” in (a), and “painting” in (b). (2) Omitting the T2T module weakens token interactions at both segment and image granularity, affecting attention. For instance, without T2T, the “boy” and “ball” relationship in “a boy playing with a beach ball” is disrupted in (c). (3) Excluding the I2I region slightly degrades alignment with the sketch, as shown in (ii) and (iv), where nearly half of the instances deviate from their sketches. Besides the visualizations, we also conduct the quantitative evaluation on different variants presented in the last three rows of Table 1. While I2T alone improves all scenarios, T2T enhances token interactions, and I2I refines sketch-to-image alignment, both boosting human preference scores. These observations align with DiT-based analysis in Section 3.2, emphasizing the essential roles of T2T, I2T, and I2I in prompt alignment.

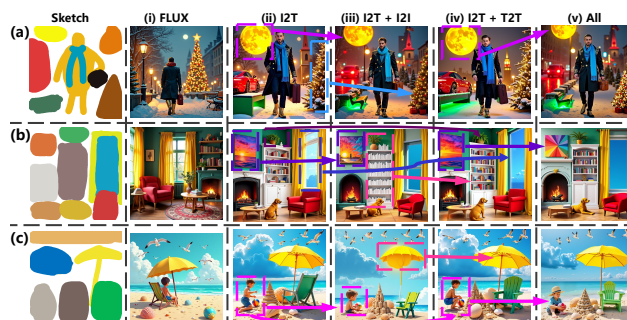


Figure 7: Ablation study on attention modules (Prompts in Figure 5). The I2T module mainly enhances layout-prompt alignment, T2T improves token interactions within segments, and I2I further refines instance self-alignment. Arrow direction indicates better. More study on hyper-parameters are in Appendix.2.

#### Analysis.

We also examine the scaling trend based on  $a \cdot \exp(\beta_t \cdot (m - a))$  of Eq. (2) with  $\lambda = 4.0$  and  $T = 32$ , considering two scenarios:  $m = 0$  and  $m = 1$ , where  $a$  represents the attention score  $[0, 1]$ . The results are shown in Figure 8. For  $m = 0$ , all attention scores are suppressed, while for  $m = 1$ , the central point ( $\sim 0.2$ ), aligns with the original range  $[0, 0.3]$ , refining the attention distribution. This phenomenon indicates that the unified scaling module suppresses less important regions and enhances key areas.

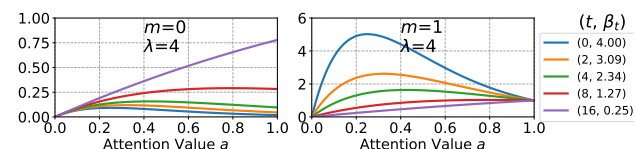


Figure 8: The scaling trend based on  $a \cdot \exp(\beta_t \cdot (m - a))$  of Eq. (2).  $m = 0$  means attenuating attention scores.  $m = 1$  means amplifying the attention score.

## 5 Conclusion

In this work, we investigated the attention mechanisms in the DiT architecture, analyzing various attention modules, and exploring the hierarchical attention responses across different tokens with step-layer-wise token exchange experiments. We proposed a training-free approach with hierarchical and step-layer-wise attention specialty tuning, enabling precise MIS using the DiT-based models. Both quantitative and qualitative evaluations on upgraded sketch-based T2I-CompBench and customized complex cases showed that our approach achieved accurate instance placement and attribute representation in detailed multi-instance layouts. Moreover, we established an analysis-design-experiment framework that can serve as a potential paradigm for future improvements in MIS.

## References

- [1] Yunji Kim, Jiyoung Lee, Jin-Hwa Kim, Jung-Woo Ha, and Jun-Yan Zhu. Dense text-to-image generation with attention modulation. In *Proceedings of the IEEE/CVF International Conference on Computer Vision*, pages 7701–7711, 2023.
- [2] Liunian Harold Li, Pengchuan Zhang, Haotian Zhang, Jianwei Yang, Chunyuan Li, Yiwu Zhong, Lijuan Wang, Lu Yuan, Lei Zhang, Jenq-Neng Hwang, et al. Grounded language-image pre-training. In *Proceedings of the IEEE/CVF Conference on Computer Vision and Pattern Recognition*, pages 10965–10975, 2022.
- [3] Yuheng Li, Haotian Liu, Qingyang Wu, Fangzhou Mu, Jianwei Yang, Jianfeng Gao, Chunyuan Li, and Yong Jae Lee. GLIGEN: Open-set grounded text-to-image generation. In *Proceedings of the IEEE/CVF Conference on Computer Vision and Pattern Recognition*, pages 22511–22521, 2023.
- [4] Guangcong Zheng, Xianpan Zhou, Xuewei Li, Zhongang Qi, Ying Shan, and Xi Li. Layoutdiffusion: Controllable diffusion model for layout-to-image generation. In *Proceedings of the IEEE/CVF Conference on Computer Vision and Pattern Recognition*, pages 22490–22499, 2023.
- [5] Zhengyuan Yang, Jianfeng Wang, Zhe Gan, Linjie Li, Kevin Lin, Chenfei Wu, Nan Duan, Zicheng Liu, Ce Liu, Michael Zeng, et al. Reco: Region-controlled text-to-image generation. In *Proceedings of the IEEE/CVF Conference on Computer Vision and Pattern Recognition*, pages 14246–14255, 2023.
- [6] Jinheng Xie, Yuexiang Li, Yawen Huang, Haozhe Liu, Wentian Zhang, Yefeng Zheng, and Mike Zheng Shou. Boxdiff: Text-to-image synthesis with training-free box-constrained diffusion. In *Proceedings of the IEEE/CVF International Conference on Computer Vision*, pages 7452–7461, 2023.
- [7] Robin Rombach, Andreas Blattmann, Dominik Lorenz, Patrick Esser, and Björn Ommer. High-resolution image synthesis with latent diffusion models. In *Proceedings of the IEEE/CVF Conference on Computer Vision and Pattern Recognition*, pages 10684–10695, 2022.
- [8] Dustin Podell, Zion English, Kyle Lacey, Andreas Blattmann, Tim Dockhorn, Jonas Müller, Joe Penna, and Robin Rombach. Sdxl: Improving latent diffusion models for high-resolution image synthesis. *arXiv preprint arXiv:2307.01952*, 2023.
- [9] Long Lian, Boyi Li, Adam Yala, and Trevor Darrell. LLM-grounded diffusion: Enhancing prompt understanding of text-to-image diffusion models with large language models. *arXiv preprint arXiv:2305.13655*, 2023.
- [10] Dwei Zhou, You Li, Fan Ma, Xiaoting Zhang, and Yi Yang. MIGC: Multi-instance generation controller for text-to-image synthesis. In *Proceedings of the IEEE/CVF Conference on Computer Vision and Pattern Recognition*, pages 6818–6828, 2024.
- [11] Zhenhong Sun, Junyan Wang, Zhiyu Tan, Daoyi Dong, Hailan Ma, Hao Li, and Dong Gong. EGGGen: Image generation with multi-entity prior learning through entity guidance. In *Proceedings of the 32nd ACM International Conference on Multimedia*, page 6637–6645, 2024.
- [12] Quynh Phung, Songwei Ge, and Jia-Bin Huang. Grounded text-to-image synthesis with attention refocusing. In *Proceedings of the IEEE/CVF Conference on Computer Vision and Pattern Recognition*, pages 7932–7942, 2024.
- [13] Minghao Chen, Iro Laina, and Andrea Vedaldi. Training-free layout control with cross-attention guidance. In *Proceedings of the IEEE/CVF Winter Conference on Applications of Computer Vision*, pages 5343–5353, 2024.
- [14] Ling Yang, Zhaochen Yu, Chenlin Meng, Minkai Xu, Stefano Ermon, and CUI Bin. Mastering text-to-image diffusion: Recapturing, planning, and generating with multimodal LLMs. In *Forty-first International Conference on Machine Learning*, 2024.
- [15] Jaskirat Singh, Jianming Zhang, Qing Liu, Cameron Smith, Zhe Lin, and Liang Zheng. Smartmask: Context aware high-fidelity mask generation for fine-grained object insertion and layout control. In *Proceedings of the IEEE/CVF Conference on Computer Vision and Pattern Recognition*, pages 6497–6506, 2024.

- [16] Kuan Heng Lin, Sicheng Mo, Ben Klingher, Fangzhou Mu, and Bolei Zhou. Ctrl-x: Controlling structure and appearance for text-to-image generation without guidance. *arXiv preprint arXiv:2406.07540*, 2024.
- [17] Xudong Wang, Trevor Darrell, Sai Saketh Rambhatla, Rohit Girdhar, and Ishan Misra. Instancediffusion: Instance-level control for image generation. In *Proceedings of the IEEE/CVF Conference on Computer Vision and Pattern Recognition*, pages 6232–6242, 2024.
- [18] Black Forest Labs. Flux. <https://github.com/black-forest-labs/flux>, 2024. Initial commit on August 1, 2024, Accessed: 2024-10-31.
- [19] Patrick Esser, Sumith Kulal, Andreas Blattmann, Rahim Entezari, Jonas Müller, Harry Saini, Yam Levi, Dominik Lorenz, Axel Sauer, Frederic Boesel, et al. Scaling rectified flow transformers for high-resolution image synthesis. In *Forty-first International Conference on Machine Learning*, 2024.
- [20] William Peebles and Saining Xie. Scalable diffusion models with transformers. In *Proceedings of the IEEE/CVF International Conference on Computer Vision*, pages 4195–4205, 2023.
- [21] Kaiyi Huang, Kaiyue Sun, Enze Xie, Zhenguo Li, and Xihui Liu. T2I-CompBench: A comprehensive benchmark for open-world compositional text-to-image generation. In A. Oh, T. Naumann, A. Globerson, K. Saenko, M. Hardt, and S. Levine, editors, *Advances in Neural Information Processing Systems*, volume 36, pages 78723–78747. Curran Associates, Inc., 2023.
- [22] Jascha Sohl-Dickstein, Eric Weiss, Niru Maheswaranathan, and Surya Ganguli. Deep unsupervised learning using nonequilibrium thermodynamics. In *International Conference on Machine Learning*, pages 2256–2265. PMLR, 2015.
- [23] Yang Song and Stefano Ermon. Generative modeling by estimating gradients of the data distribution. *Advances in Neural Information Processing Systems*, 32, 2019.
- [24] Jonathan Ho, Ajay Jain, and Pieter Abbeel. Denoising diffusion probabilistic models. *Advances in Neural Information Processing Systems*, 33:6840–6851, 2020.
- [25] Jiaming Song, Chenlin Meng, and Stefano Ermon. Denoising diffusion implicit models. *arXiv preprint arXiv:2010.02502*, 2020.
- [26] Florinel-Alin Croitoru, Vlad Hondru, Radu Tudor Ionescu, and Mubarak Shah. Diffusion models in vision: A survey. *IEEE Transactions on Pattern Analysis and Machine Intelligence*, 45(9):10850–10869, 2023.
- [27] Alex Nichol, Prafulla Dhariwal, Aditya Ramesh, Pranav Shyam, Pamela Mishkin, Bob McGrew, Ilya Sutskever, and Mark Chen. GLIDE: Towards photorealistic image generation and editing with text-guided diffusion models. *arXiv preprint arXiv:2112.10741*, 2021.
- [28] Chitwan Saharia, William Chan, Saurabh Saxena, Lala Li, Jay Whang, Emily L Denton, Kamyar Ghasemipour, Raphael Gontijo Lopes, Burcu Karagol Ayan, Tim Salimans, et al. Photorealistic text-to-image diffusion models with deep language understanding. *Advances in Neural Information Processing Systems*, 35:36479–36494, 2022.
- [29] Diederik P Kingma. Auto-encoding variational Bayes. *arXiv preprint arXiv:1312.6114*, 2013.
- [30] Olaf Ronneberger, Philipp Fischer, and Thomas Brox. U-net: Convolutional networks for biomedical image segmentation. In *International Conference on Medical Image Computing and Computer-Assisted Intervention*, pages 234–241. Springer, 2015.
- [31] Junsong Chen, Jincheng Yu, Chongjian Ge, Lewei Yao, Enze Xie, Yue Wu, Zhongdao Wang, James Kwok, Ping Luo, Huchuan Lu, et al. Pixart- $\alpha$ : Fast training of diffusion transformer for photorealistic text-to-image synthesis. *arXiv preprint arXiv:2310.00426*, 2023.
- [32] Nanye Ma, Mark Goldstein, Michael S Albergo, Nicholas M Boffi, Eric Vanden-Eijnden, and Saining Xie. SiT: Exploring flow and diffusion-based generative models with scalable interpolant transformers. *arXiv preprint arXiv:2401.08740*, 2024.
- [33] Xingchao Liu, Chengyue Gong, and Qiang Liu. Flow straight and fast: Learning to generate and transfer data with rectified flow. *arXiv preprint arXiv:2209.03003*, 2022.
- [34] Qiucheng Wu, Yujian Liu, Handong Zhao, Trung Bui, Zhe Lin, Yang Zhang, and Shiyu Chang. Harnessing the spatial-temporal attention of diffusion models for high-fidelity text-to-image synthesis. In *Proceedings of the IEEE/CVF International Conference on Computer Vision*, pages 7766–7776, 2023.
- [35] Zhenhong Sun, Yifu Wang, Yonhon Ng, Yunfei Duan, Daoyi Dong, Hongdong Li, and Pan Ji. T<sup>3</sup>-s2s: Training-free triplet tuning for sketch to scene generation. *arXiv preprint arXiv:2412.13486*, 2024.
- [36] Xin Xie and Dong Gong. Dymo: Training-free diffusion model alignment with dynamic multi-objective scheduling. In *Proceedings of the IEEE/CVF Conference on Computer Vision and Pattern Recognition (CVPR)*, June 2025.

- [37] Amir Hertz, Ron Mokady, Jay Tenenbaum, Kfir Aberman, Yael Pritch, and Daniel Cohen-Or. Prompt-to-prompt image editing with cross attention control. *arXiv preprint arXiv:2208.01626*, 2022.
- [38] Weixi Feng, Xuehai He, Tsu-Jui Fu, Varun Jampani, Arjun Akula, Pradyumna Narayana, Sugato Basu, Xin Eric Wang, and William Yang Wang. Training-free structured diffusion guidance for compositional text-to-image synthesis. *arXiv preprint arXiv:2212.05032*, 2022.
- [39] Nataniel Ruiz, Yuanzhen Li, Varun Jampani, Yael Pritch, Michael Rubinstein, and Kfir Aberman. DreamBooth: Fine tuning text-to-image diffusion models for subject-driven generation. In *Proceedings of the IEEE/CVF conference on Computer Vision and Pattern Recognition*, pages 22500–22510, 2023.
- [40] Yupeng Zhou, Daquan Zhou, Zuo-Liang Zhu, Yaxing Wang, Qibin Hou, and Jiashi Feng. Maskdiffusion: Boosting text-to-image consistency with conditional mask. *arXiv preprint arXiv:2309.04399*, 2023.
- [41] Susung Hong, Gyuseong Lee, Wooseok Jang, and Seungryong Kim. Improving sample quality of diffusion models using self-attention guidance. In *Proceedings of the IEEE/CVF International Conference on Computer Vision*, pages 7462–7471, 2023.
- [42] Junyan Wang, Zhenhong Sun, Zhiyu Tan, Xuanbai Chen, Weihua Chen, Hao Li, Cheng Zhang, and Yang Song. Towards effective usage of human-centric priors in diffusion models for text-based human image generation. In *Proceedings of the IEEE/CVF Conference on Computer Vision and Pattern Recognition*, pages 8446–8455, 2024.
- [43] Andrey Voynov, Qinghao Chu, Daniel Cohen-Or, and Kfir Aberman. P+: Extended textual conditioning in text-to-image generation. *arXiv preprint arXiv:2303.09522*, 2023.
- [44] Jiazheng Xu, Xiao Liu, Yuchen Wu, Yuxuan Tong, Qinkai Li, Ming Ding, Jie Tang, and Yuxiao Dong. ImageReward: Learning and evaluating human preferences for text-to-image generation. *Advances in Neural Information Processing Systems*, 36:15903–15935, 2023.
- [45] Bo Cheng, Yuhang Ma, Liebucha Wu, Shanyuan Liu, Ao Ma, Xiaoyu Wu, Dawei Leng, and Yuhui Yin. HiCo: Hierarchical controllable diffusion model for layout-to-image generation. *arXiv preprint arXiv:2410.14324*, 2024.
- [46] Jiayu Xiao, Henglei Lv, Liang Li, Shuhui Wang, and Qingming Huang. RnB: Region and boundary aware zero-shot grounded text-to-image generation. *arXiv preprint arXiv:2310.08872*, 2023.
- [47] Phillip Y Lee, Taehoon Yoon, and Minhyuk Sung. GrounDiT: Grounding diffusion transformers via noisy patch transplantation. *arXiv preprint arXiv:2410.20474*, 2024.
- [48] OpenAI, Josh Achiam, Steven Adler, Sandhini Agarwal, et al. Gpt-4 technical report, 2024.
- [49] Kaiyi Huang, Kaiyue Sun, Enze Xie, Zhenguo Li, and Xihui Liu. T2I-CompBench: A comprehensive benchmark for open-world compositional text-to-image generation. In *Thirty-seventh Conference on Neural Information Processing Systems Datasets and Benchmarks Track*, 2023.
- [50] Junnan Li, Dongxu Li, Caiming Xiong, and Steven Hoi. BLIP: Bootstrapping language-image pre-training for unified vision-language understanding and generation. In Kamalika Chaudhuri, Stefanie Jegelka, Le Song, Csaba Szepesvari, Gang Niu, and Sivan Sabato, editors, *Proceedings of the 39th International Conference on Machine Learning*, volume 162 of *Proceedings of Machine Learning Research*, pages 12888–12900. PMLR, 17–23 Jul 2022.
- [51] Xingyi Zhou, Vladlen Koltun, and Philipp Krähenbühl. Simple multi-dataset detection. In *Proceedings of the IEEE/CVF Conference on Computer Vision and Pattern Recognition*, pages 7571–7580, June 2022.
- [52] Jack Hessel, Ari Holtzman, Maxwell Forbes, Ronan Le Bras, and Yejin Choi. CLIPScore: A reference-free evaluation metric for image captioning. *arXiv preprint arXiv:2104.08718*, 2021.
- [53] RIR BT. Methodology for the subjective assessment of the quality of television pictures. *International Telecommunication Union*, 4:19, 2007.
- [54] Mingjian Zhu, Hanting Chen, Qiangyu YAN, Xudong Huang, Guanyu Lin, Wei Li, Zhijun Tu, Hailin Hu, Jie Hu, and Yunhe Wang. GenImage: A million-scale benchmark for detecting AI-generated image. In *Advances in Neural Information Processing Systems*, volume 36, pages 77771–77782, 2023.
- [55] David C. Epstein, Ishan Jain, Oliver Wang, and Richard Zhang. Online detection of AI-generated images. In *Proceedings of the IEEE/CVF International Conference on Computer Vision Workshops*, pages 382–392, October 2023.
- [56] Zhendong Wang, Jianmin Bao, Wengang Zhou, Weilun Wang, Hezhen Hu, Hong Chen, and Houqiang Li. DIRE for diffusion-generated image detection. In *Proceedings of the IEEE/CVF International Conference on Computer Vision*, pages 22445–22455, October 2023.



Figure 9: Ablation on step-layer-wise tuning. Full-layer tuning: adding tuning across all layers with varying  $[\lambda_{cross}, \lambda_{self}]$  degrades image quality, leading to instance repetition, over-saturation, and distortion due to disrupted attention responses.

## SUPPLEMENTARY MATERIALS

### 1 Ethical and Social Impacts

This study on MIS in DiT, which incorporates AST and HSLW modules and builds on the FLUX and SD v3.5 base models from the HuggingFace diffusers library [18], assesses performance on the widely used T2I-CompBench datasets [21] and raises several ethical and societal implications. Primary among these is the privacy preservation challenge in synthetic media generation, as the model’s capability to synthesize multi-instance compositions from textual descriptions potentially enables the unauthorized reproduction of individual likenesses, necessitating robust privacy-preserving mechanisms. In addition, the underlying FLUX and SD v3.5 architectures exhibit inherent representational biases that can manifest themselves in stereotypical image generation, requiring continuous bias monitoring and mitigation strategies to ensure equitable representation. While our methodology advances diverse multi-instance figure generation, it also poses risks regarding the creation of synthetic media for malicious purposes. This research demonstrates that advancing DiT capabilities must be accompanied by rigorous ethical considerations, particularly in privacy preservation, bias mitigation, and the establishment of safeguards against misuse in multi-instance figure synthesis.

### 2 Hyper-Parameters $\lambda$ and Layer Comparison

In this section, we systematically investigate the impact of two critical design elements: the hyper-parameters  $(\lambda_{self}, \lambda_{cross})$  in the AST module and our proposed HSLW optimization strategy. First, we conduct thorough experiments to determine optimal hyper-parameter  $(\lambda_{self}, \lambda_{cross})$  in the AST module, formalized in Eq. (2) of the main text, and configurations for MIS. Through empirical analysis of both symmetrical parameter pairs  $[(0.1, 0.1), (0.5, 0.5), (1, 1), (2, 2)]$  and asymmetric configurations  $[(1, 5), (2, 5), (3, 1)-(3, 5)]$ , we demonstrate that the optimal parameter combination (3.5, 5) achieves superior synthesis quality. As shown in Figure 10, this configuration maintains precise instance localization while ensuring visual coherence.

To validate the necessity of our HSLW module, we conduct a comparative full-layer tuning experiment with results shown in Figure 9. The full-layer tuning behaves as an over-manipulation of the attention map, causing significant distortion in both foreground and background. With different parameters, the visualization results reveal several issues, including instance repetition (“painting” in (b) and “sandcastle” in (c)), missing instances (“green bench” in (a) and “blue cloud” in (c)), attribute leakage (“green plant” in (b)), and inaccurate placement across all three cases. These suboptimal results confirm the effectiveness of our layer-tuning strategy, which tunes the attention map via specific masks across different diffusion phases, enhancing coherence and accuracy.



Figure 10: The visualization comparison with different hyper-parameters ( $\lambda_{self}$ ,  $\lambda_{cross}$ ) on complex MIS. The results of our choices present the best performance on the the instance placement and attribute representation.

### 3 Detailed Formulation of G

To compute the similarity matrix  $G$ , we first transform each binary sketch mask  $S_i \in \mathbb{R}^{h \times w}$  into a flattened vector representation  $\bar{S}_i \in \mathbb{R}^{hw \times 1}$ . Given a batch of sketch masks, we construct an intermediate correlation matrix  $L \in \mathbb{R}^{hw \times hw}$  through batch-wise outer products:

$$L = \sum_{i=1}^{batch} \bar{S}_i \bar{S}_i^T \quad (6)$$

The sensitivity matrix  $G \in \mathbb{R}^{hw \times 1}$  is then computed by normalizing and scaling  $L$ :

$$G = 1 - \gamma \frac{\sum_{i=1}^{hw} L_i}{hw} \quad (7)$$

where  $\gamma$  is a modality-dependent scaling factor set to 4.0 for text queries and 1.0 for image queries. This formulation guarantees that  $G$  captures the pairwise relationships between spatial locations while taking into account the characteristics specific to the modality.

### 4 Module Comparison on SD v3.5 Model

To validate the general applicability of our HSLW module beyond the FLUX model, we apply our approach to another flow-matching DiT-based model, Stable Diffusion 3.5 (SD v3.5) [19]. Since SD v3.5 may exhibit step- and layer-specific behavior across its four attention areas, we implement the same HSLW attention tuning strategy during the first half of the steps for effective validation. SD v3.5 concatenates text embeddings from CLIP and T5 tokenizers, resulting in



Figure 11: Visualizations for transferring our approach to the SD v3.5 model [19]. The corresponding prompts are also shown in Figure 5 in the main text and more are shown by Figures 21-23 in Appendix.5. We present two implementation variants: The first variant integrates the AST module with a full-layer tuning strategy, i.e., SD v3.5+All Layers Tuning, whereas the second variant combines the AST module with a HSLW tuning strategy while retaining the default configuration, i.e., Ours+SD v3.5. When implemented on SD v3.5, our framework achieves precise multi-instance alignment between textual prompts and spatial layouts, as shown by the visualization results. The underlined prompts within the prompts are the sub-prompts for instances, with colors matching those in the sketch.

two corresponding T2I and T2T masks per tokenizer, applied as outlined in Figure 4 of the main text. Using the same prompts and sketches as in Figure 5 of the main text, we adopt the same hyperparameters except for  $(\lambda_{self}, \lambda_{cross})$ , adjusted to avoid over-manipulation of the attention maps. As demonstrated in Figure 11, HSLW module significantly improves sketch-image alignment compared to standalone AST modules, while preserving prompt consistency across multi-instance scenarios. This confirms the model-agnostic compatibility of AST+HSLW modules with flow-matching DiT-based models, achieving performance comparable to FLUX-dev implementations. Future research will investigate independent HSLW applications to both CLIP- and T5-derived attention maps. Despite these limitations, the results indicate effective generalization and potential for advancing future flow-matching DiT-based models.

## 5 Upgraded Sketch of T2I-CompBench

Our method requires preliminary sketch information, which we obtain using GPT-4V [48], a most-recent language-vision model. GPT-4V creates sketch images by automatically segmenting each instance and outputting the corresponding sketch mask based on a textual description of the desired scene. To maintain proper spatial layouts and relationships, all generated sketch images are manually refined. The sketch source, including the GPT-4V generated sketches and their manually adjusted counterparts, will be accessible upon the release of the main code.

Meanwhile, using T2I-CompBench evaluation metrics, i.e., B-VQA [50], UniDet [51], and CLIP-Score [52], all yield scores of 0 (range: 0 to 1, with 1 being best), resulting our method showing a slight increase in Table 1 of the main paper. To illustrate this failure, we randomly select six cases (three spatial, three color) displayed in Figure 20. Upon manual inspection of the images generated from T2I-CompBench prompts, most comply with the attribute representation and layout constraints. The problem arises from a distribution mismatch: these evaluation tools were trained on data significantly different from our generated images, resulting in lower T2I-CompBench scores [54]. This failure of pre-trained models to effectively process generated images is well-documented [55, 56]. Therefore, we also designed more customized complex cases to evaluate image quality in the next section.



Figure 12: Comparison with attention modulation before/after softmax. Applying the unified scaling module to the attention map after softmax effectively enhances alignment between prompts and sketch masks.

## 6 Customized Complex Cases

To evaluate the overall image quality, we customized 20 complex scenes containing 6-8 instances and invited the participants to evaluate our prompt-generated image pairs under the guidelines of the multimedia subjective testing [53] from the perspective of prompt-image alignment, sketch/layout-to-image coherence, aesthetic preference. Each case specifies more than 6 distinct instances with unique attributes. As depicted in Figures 21-23, our method produces multiple instances with their designated attributes more accurately, cohesively integrating background and foreground elements while adhering to the sketch constraints. The misalignment between the textual description and the prior sketch information in the other models leads to these limitations.

We implement a pipeline for systematic assessment: (1) Fair Generation: For each of 20 complex scenes, each method generates 20 images with random seeds. (2) Random Sampling: From each scene-method pair’s 20 variants, we randomly select one evaluation instance. (3) Blinded Assessment: All selected samples are aggregated and presented in randomized order, preventing positional bias during assessment. For the evaluation, we require the participants to consider the explicit spatial relationship between segments regarding the layout. To be specific, the criteria for overall assessment could be summarized as:

- **5:** Alignment with both layout and textual prompts. All elements are correctly placed with high quality (sharp details, proper proportions, no artifacts).
- **4:** Minor discrepancies in 1 element missing or misplacing, or slight quality degradation (blurring/mild distortion) in one component.
- **3:** More errors in 2 elements omissions or misplacements, or moderate quality issues (visible distortion/partial incoherence).
- **2:** More than 3 placement inaccuracies, or errors affecting more than 2 elements with quality flaws (severe distortions/unnatural blending).
- **1:** More than 4 errors elements missing or severely misplaced with low-quality rendering (fragmented objects/unrecognizable shapes).

## 7 AST Module Before and After Softmax

To validate our AST module, which modulates the attention map after softmax, we qualitatively compare the visualization results with the attention modulation method in Dense Diffusion as shown in Eq. (2) [1]. The visualization results are provided in Figure 12. These results indicate that attention modulation before softmax presents several issues, including incorrect instances (“scarf” in (a) and “yellow umbrella” in (c)), missing instances (“green bench” in (a) and “golden dog” in (b)), inaccurate attributes (“blue cloud” in (c)), and misplacement in all three cases. These suboptimal outcomes validate our AST strategy, which modulates the attention map after softmax, enhancing the coherence and accuracy of MIS.



## 8 More Attention Analysis

### 8.1 Analysis of T2I Attention Map

This part presents the T2I maps from Section 3.2, which were omitted from the main text due to space constraints. These maps are depicted in Figure 13. In comparison to other attention modules, T2I maps exhibit significantly lower attention scores and contain limited semantic information, resulting in a weak influence on the overall attention map. In conclusion, while T2I maps could slightly improve text responsiveness, they significantly increase computational burden and are therefore not incorporated into our method.

### 8.2 More Attention Analysis of FLUX-dev

We observed similar patterns in attention maps across multiple instances, but we only include one prompt example in the main paper due to space constraints. Here, we provide additional map analysis in the full paper, focusing on the prompt “Yellow orb in cave” to systematically assess four attention regions within the FLUX framework. The visualization maps are categorized by types as shown in Figure 15: self-attention maps (T2T and I2I), and cross-attention-based I2T and T2I maps, supporting the consistent findings presented in Figure 2 of the main paper. Additionally, we performed a t-SNE analysis of attention maps across different text prompts, as demonstrated below.

### 8.3 t-SNE Analysis of Attention

To comprehensively analyze the attention mechanism in the FLUX model, we conducted experiments using diverse textual prompts and performed statistical analysis of attention responses across multiple samples. Specifically, we employed GPT-4 to generate 512 structured prompts in the format “[color] [Instance] in [Background]” to ensure systematic coverage of variations. For a detailed investigation of attention response patterns, we extracted statistical summaries by aggregating attention maps across three key layer ranges (6-10, 20-24, and 50-54) in the first 16 steps. These layer ranges were chosen based on preliminary analysis of attention distribution in Section 3.2. We then applied t-SNE dimensionality reduction to visualize and analyze the characteristic patterns of attention responses, enabling robust verification of our findings regarding the attention distribution across different components of prompts. The results of the t-SNE analysis on three chosen layers are displayed in Figure 14. In the shallow layers (6-10), instances exhibit a more aggregated pattern, while attributes and backgrounds display a more dispersed distribution. This highlights the significance of instances in these layers. In the middle layers (20-24), all three classes—instances, attributes, and backgrounds—are more dispersed from each other, with no clear aggregation. This suggests a considerable interplay among them. Interestingly, while the background tends to group in other layers, it becomes more intertwined with other elements in the middle layers, confirming that background control has varied effects at this stage. In the deep layers (50-54), the separation and aggregation of backgrounds and instances become more evident, alongside a strong coupling between attributes and instances. This indicates that attributes are crucial in the later stages.

### 8.4 Attention Analysis of FLUX-schnell

Following the same analytical process in Section 3.2, we employ the prompt “Red cube in a forest” to examine the functionality of four regions in the attention maps of the FLUX-schnell model. The visualization maps are categorized by types, as depicted in Figure 16, confirming the observations made in the FLUX-dev model analysis.

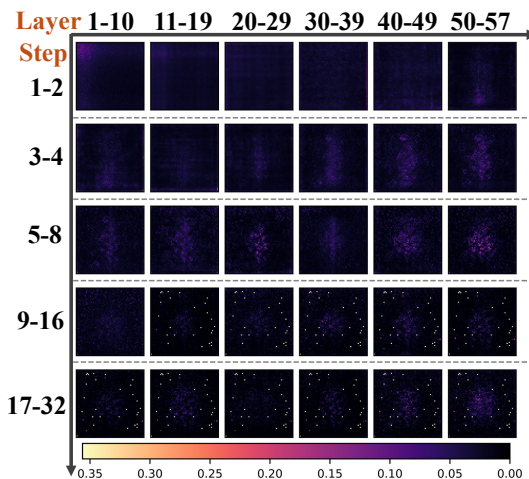


Figure 13: The T2I average attention maps omitted in Section 3.2. Compared to other attention maps, T2I maps exhibit lower scores, indicating a weak impact, and consequently, they are not modulated by our AST module.

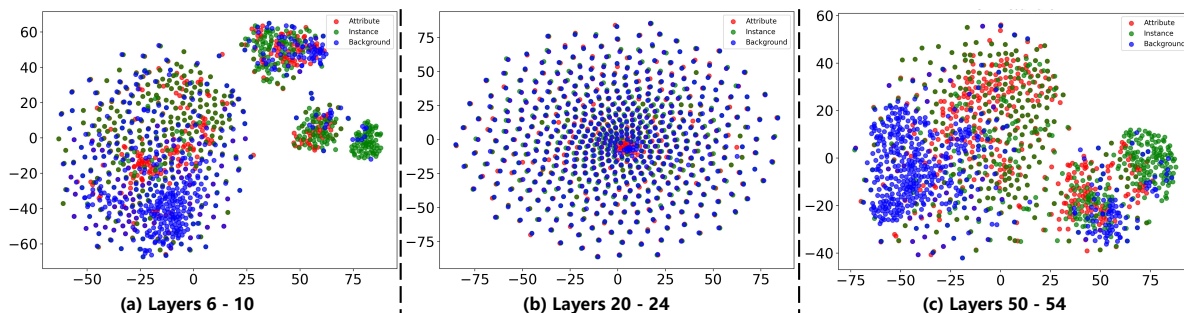


Figure 14: Systematic analysis of Flux model’s attention mechanisms using 512 GPT-4-generated structured prompts (“[color][instance] in [background]”), e.g., “Green pyramid in the ocean”, “Yellow cone in the mountain”, and “Purple cylinder in the river”. In the shallow layers (6-10), instances exhibit a more aggregated pattern, with attributes and backgrounds displaying a more dispersed distribution. This highlights the importance of instances in these layers. In the middle layers (20-24), all three classes—instances, attributes, and backgrounds—are more dispersed from each other, with no clear aggregation. This suggests a significant interplay between them. Notably, while the background tends to aggregate in other layers, it becomes more intertwined with other elements in the middle layers, confirming that background control has varied effects at this stage. In the deep layers (50-54), the separation and aggregation of backgrounds and instances become more pronounced, alongside the strong coupling between attributes and instances. This indicates that attributes play a crucial role in the later stages.

## 9 Details of Token Exchanging Experiments

To further substantiate the findings and conclusions in Section 3.2 of the main text, we conducted three systematic token-exchange experiments. The experimental design utilized the following prompt pairs: (1) “Red cube in a forest” and “Blue car in indoor parking”, (2) “Yellow dish in a kitchen” and “White chair in a playground”, and (3) “Orange cone in a street” and “Green cylinder on a rooftop”. The comprehensive results of these token exchanges are visually documented in Figures 17-19. The model demonstrates remarkable responsiveness in early stages (by step 8), as shown by the seamless integration of color components (“Red”, “Orange”, “Yellow”), object instances (“cube”, “cone”, “dish”), and background contexts (“forest”, “street”, “kitchen”). Selective replacements of components, such as color, instance, and background, function on different layers, further confirming our prior conclusions on attention map analysis in Section 3.2. These findings enhance confidence for developing our HSLW module on the FLUX model for controllable MIS with complex prompts and specific layouts.

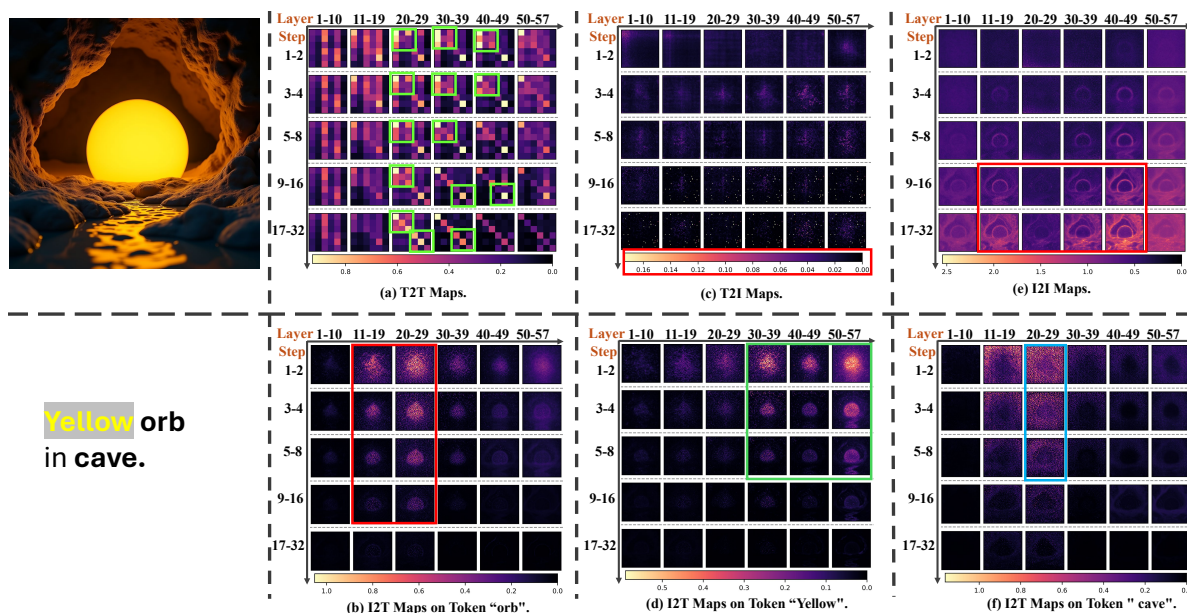


Figure 15: Attention map of the FLUX-dev model averages for the prompt “Yellow orb in cave.”, which strengthens our findings in Section 3.2. (a) T2T maps show strong intra-segment interactions within valid tokens of “Yellow orb” (first 3 tokens) and “cave” (last 2 tokens). (b) I2I maps (the maximum value of each point relative to all other points) reveal consistent interaction between “Yellow orb” and “cave” in the middle layers of four steps. (c) T2I maps show lower scores relative to others, indicating a weak impact. (d/e/f) I2T attention maps on individual tokens highlight that instance tokens dominate early layers, background tokens in the middle, and color tokens later, with most information integrated in the first half of steps.

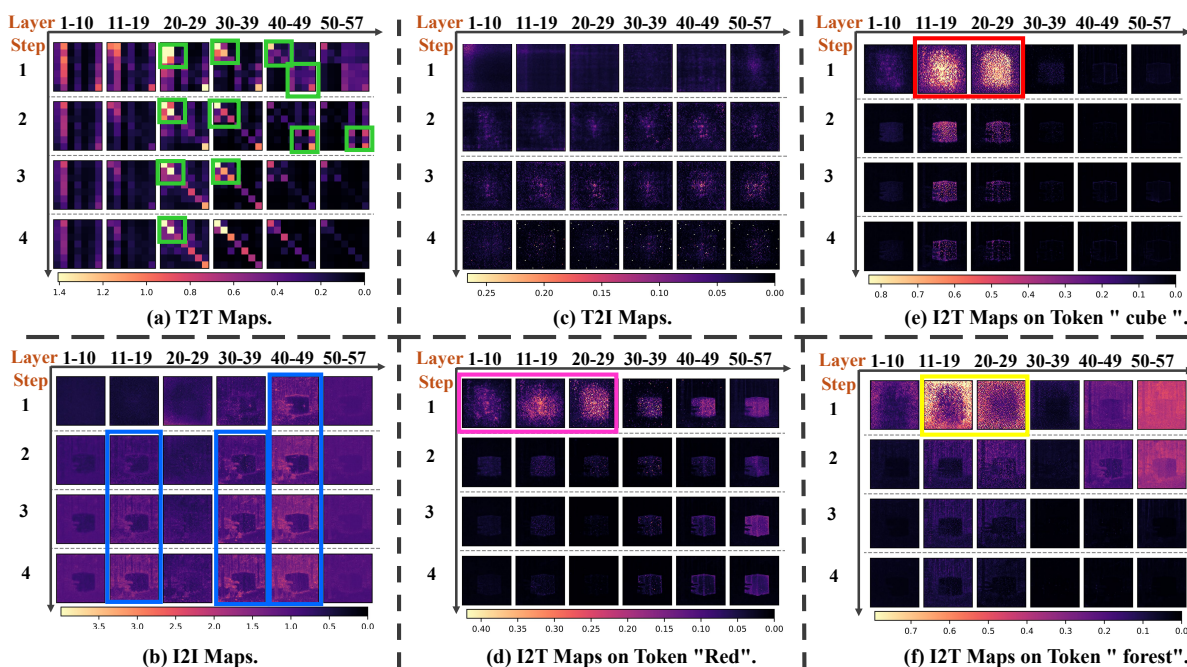


Figure 16: Attention map of the FLUX-schnell model averages for the prompt “Red cube in a forest”, which illustrates similar findings to the FLUX-dev model in Section 3.2. (a) T2T maps show strong intra-segment interactions within valid tokens of “Red cube” (first 3 tokens) and “in a forest” (last 4 tokens). (b) I2I maps (the maximum value of each point relative to all other points) reveal consistent interaction between “Red cube” and “a forest” in the middle layers of four steps. (c) T2I maps show lower scores relative to others, indicating a weak impact. (d/e/f) I2T attention maps on individual tokens highlight that instance, background, and color tokens all dominate in the left half layers of the first step.

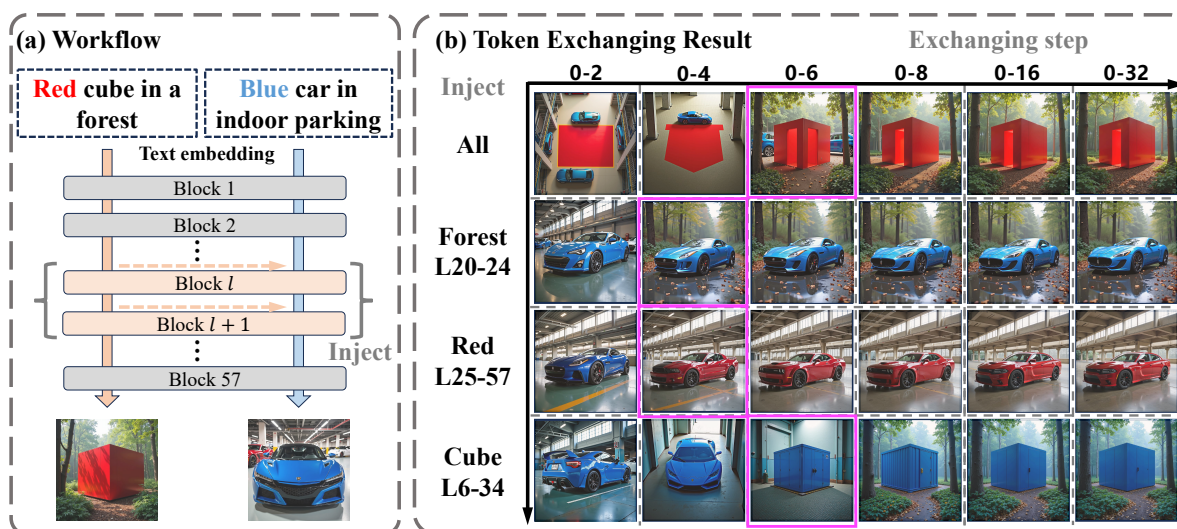


Figure 17: Token exchanging experiment between the prompts “Red cube in a forest” and “Blue car in indoor parking” (a) In a single batch, we exchange the token-specific elements of the text embedding between the left and right sides at specific layers and steps. (b) Results reveal that during the initial 8 steps, it is possible to selectively replace specific token components at certain layers. These controlled exchanges support the hierarchical attention response patterns observed in Figure 2 of the main text, providing further evidence for the model’s ability to handle fine-grained manipulations.

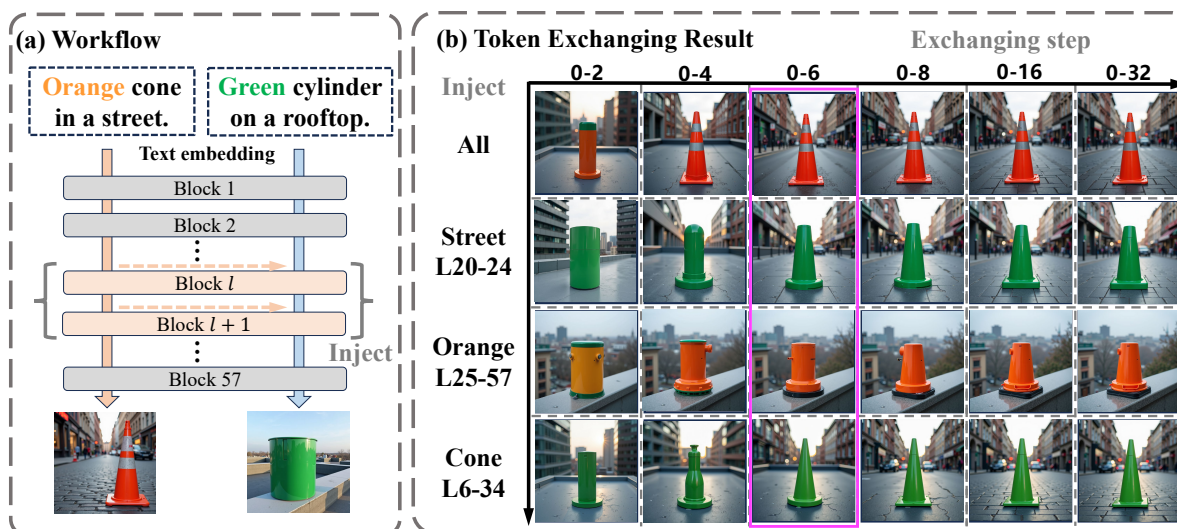


Figure 18: Token exchanging experiment between the prompts “Orange cone in a street” and “Green cylinder on a rooftop”. (a) In a single batch, we exchange the token-specific elements of the text embedding between the left and right sides at specific layers and steps. (b) Results reveal that during the initial 8 steps, it is possible to selectively replace specific token components at certain layers. These controlled exchanges support the hierarchical attention response patterns observed in Figure 2 of the main text, providing further evidence for the model’s ability to handle fine-grained manipulations.

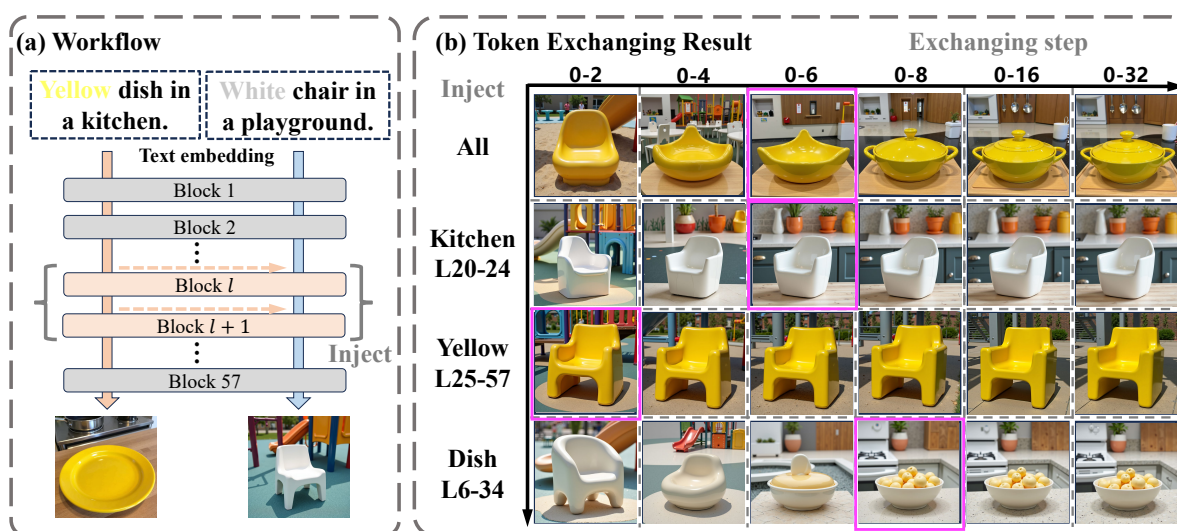


Figure 19: Token exchanging experiment between the prompts “Yellow dish in a kitchen” and “White chair in a playground”. (a) Within the same batch, we swap the token-specific components of the left side’s text embedding with their right-side counterparts at designated layers and steps. (b) Findings indicate that specific token components can be strategically substituted at designated layers within the first 8 steps. These targeted replacements corroborate the hierarchical attention responses depicted in Figure 2 of the main text, reinforcing the model’s capacity for precise control.

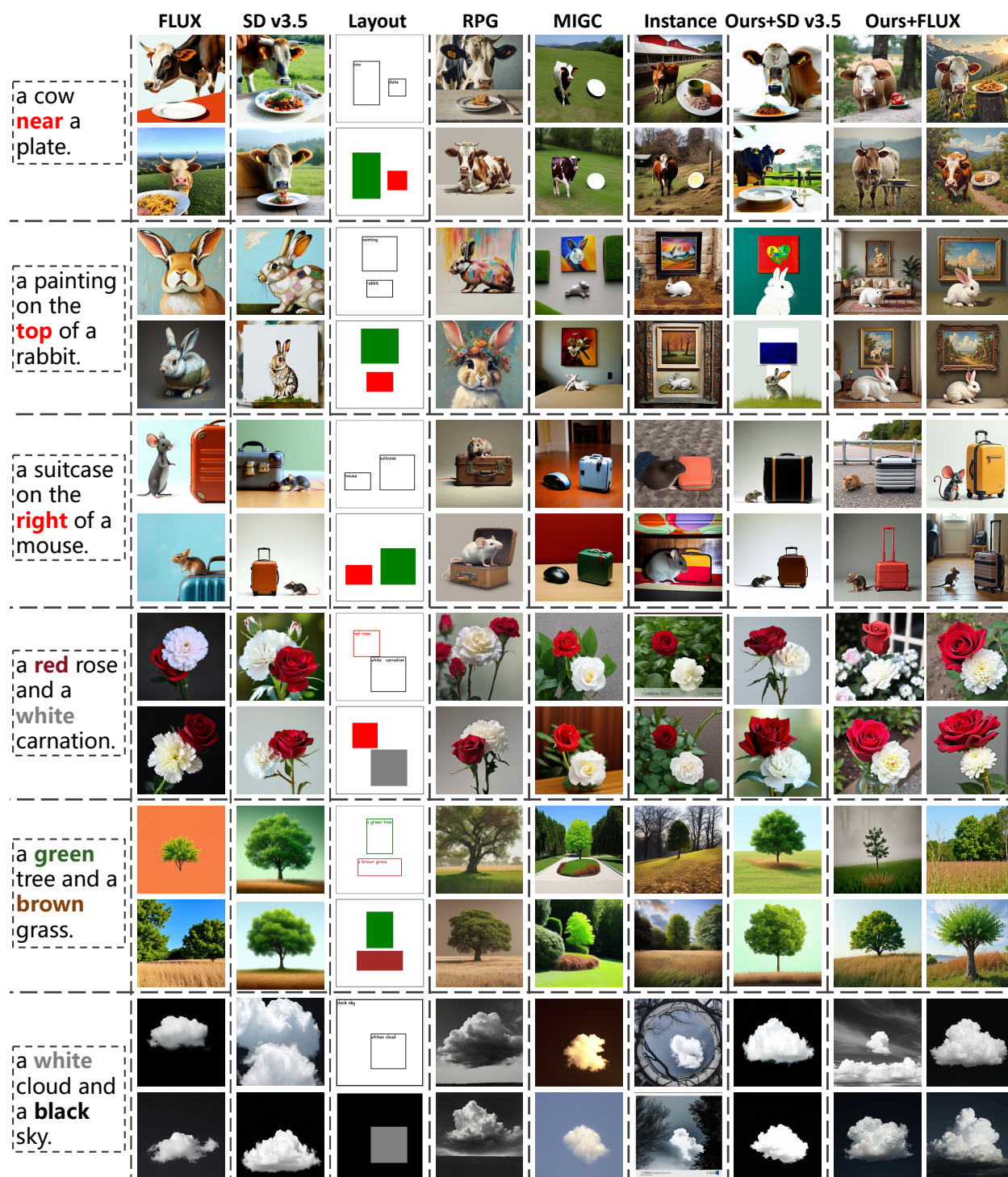


Figure 20: Comparison with other diffusion models on six T2I-CompBench. Although our method has achieved accurate instance placement, attribute representation, and enhanced diversity and realism in image quality, these generated images all received a zero score instead of the correct score. These failure cases (at least 10% in each category) contribute to our relatively low performance in the T2I-CompBench, which also indicates that a more comprehensive and powerful benchmark is required for the current text-to-image diffusion models, whose data distribution greatly deviates from the training distribution of the T2I-CompBench evaluation tools used.



Figure 21: Comparison of 7 cases with other diffusion models, supplementing the main result (Figure 5 in the main text). Bounding box layouts are provided for MIGC [10] and InstanceDiffusion [17], while the layout for RPG [14] is generated by GPT-4 [48]. Our approach uses sketch layouts and, based on the FLUX model, achieves higher multi-instance alignment with prompts and layouts. The underlined prompts within the prompts are the sub-prompts for instances, with colors matching those in the sketch.

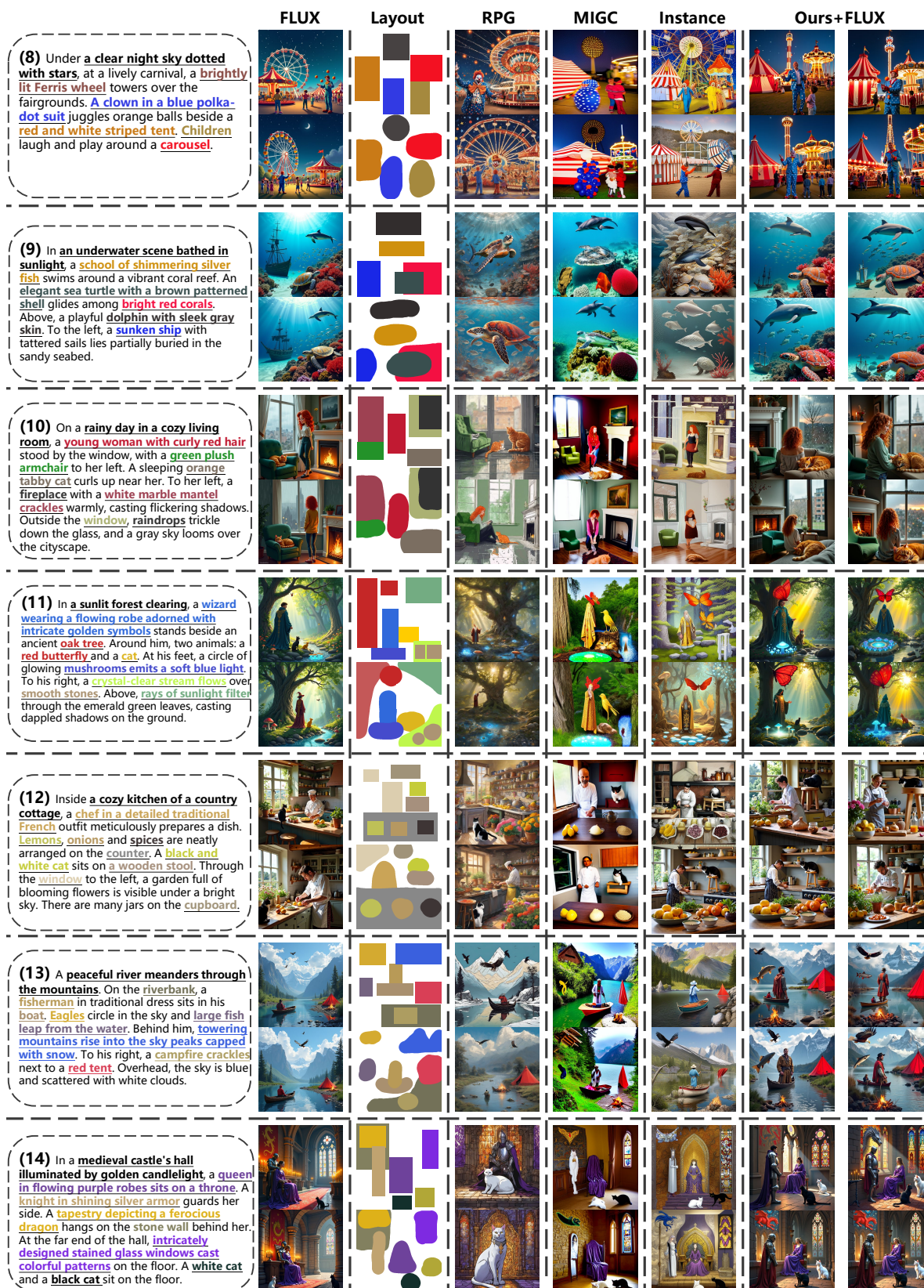


Figure 22: Comparison of 7 cases with other diffusion models, supplementing the main result (Figure 5 in the main text). Bounding box layouts are provided for MIGC [10] and InstanceDiffusion [17], while the layout for RPG [14] is generated by GPT-4 [48]. Our approach uses sketch layouts and, based on the FLUX model, achieves higher multi-instance alignment with prompts and layouts. The underlined prompts within the prompts are the sub-prompts for instances, with colors matching those in the sketch.





Figure 23: Comparison of 6 cases with other diffusion models, supplementing the main result (Figure 5 in the main text). Bounding box layouts are provided for MIGC [10] and InstanceDiffusion [17], while the layout for RPG [14] is generated by GPT-4 [48]. Our approach uses sketch layouts and, based on the FLUX model, achieving higher multi-instance alignment with prompts and layouts. The underlined prompts within the prompts are the sub-prompts for instances, with colors matching those in the sketch.